Hindawi
Geofluids
Volume 2018, Article ID 2973181, 12 pages
https://doi.org/10.1155/2018/2973181

Research Article

Theoretical Modeling of Dielectric Properties of Artificial Shales

Tongcheng Han,[1,2] **Roman Beloborodov**,[3] **Marina Pervukhina**,[4] **Matthew Josh**,[4] **Yanlin Cui**,[5] **and Pengyao Zhi**[6]

[1] *School of Geosciences, China University of Petroleum (East China), Qingdao 266580, China*
[2] *Laboratory for Marine Mineral Resources, Qingdao National Laboratory for Marine Science and Technology, Qingdao 266071, China*
[3] *Department of Exploration Geophysics, Curtin University, Perth, WA 6151, Australia*
[4] *CSIRO Energy, Perth, WA 6151, Australia*
[5] *Library, China University of Petroleum (East China), Qingdao 266580, China*
[6] *College of Earth Science and Engineering, Shandong University of Science of Technology, Qingdao 266590, China*

Correspondence should be addressed to Tongcheng Han; hantc@upc.edu.cn

Received 27 July 2017; Revised 18 October 2017; Accepted 9 November 2017; Published 11 January 2018

Academic Editor: Xiaohu Dong

Accurately modeling the anisotropic dielectric properties of shales is important for the interpretation of dielectric data acquired from shales as source rocks and unconventional reservoirs. We have developed a multiphase incremental model for the frequency dependent anisotropic dielectric properties of sedimentary rocks and presented an approach based on the developed model to simulate the measured anisotropic dielectric behaviors of artificial shales. The new model was built based on the theoretical basis of differential effective medium models for any number of mineral grain components aligned in any direction and was shown to be independent of the mixing order. The model incorporates the measured orientation distribution function of the clay particles to determine the shale dielectric anisotropy, and the frequency dependent dielectric behaviors of the wet clay minerals are obtained by inverting the dielectric properties of the artificial sample composed of clay and the same brine as in other artificial shales. The modeling technique combined important polarization mechanisms in the intermediate frequency range and was shown to give satisfactory fit to the measured frequency dependent anisotropic relative permittivity and conductivity of the artificial shales with varying silt contents by using a reasonable aspect ratio and constant dielectric parameters for the silt grains.

1. Introduction

Shales are the most abundant sedimentary rocks and are of increasing interest in hydrocarbon exploration worldwide as source rocks and unconventional reservoirs. Among the physical and petrophysical parameters employed for shale characterizations, the electrical and more specifically dielectric properties are one of the most direct and effective ways for the discrimination of geofluid types and concentrations as well as for the inference of their transport properties. However, for improved inversion and interpretation of the acquired shale dielectric data, a robust rock physics model that links the bulk dielectric properties of shales to those of the complex rock-forming components is essential. Such models must also be able to account for the shale anisotropy caused by the preferential orientation of mineral foliations.

In recent decades, shale dielectric modeling was mainly focused on the effects of the electrical double layer associated with clay minerals (e.g., [1–7]). Effort has been made to develop models that can explain the dependence of complex electrical conductivity on cation exchange capacity (CEC) and specific surface area (SSA), salinity and pH of the pore water, sorption of cations and organic molecules, influence of grain size, and the relationship between surface conductivity and quadrature conductivity, temperature, and water saturation. While the model is designed for isotropic shaly materials, Revil et al. [8] generalize the versatile model to the case of anisotropic shales by introducing tensorial versions of formation factor and tortuosity with the intention of quantifying the role played by kerogen on surface conductivity and quadrature conductivity. However, the model accounts only for the Stern layer (the inner portion of the electrical double

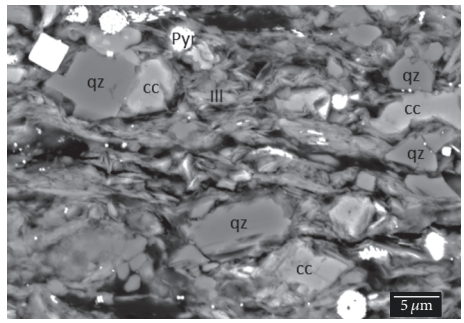

Figure 1: A scanning electron microscopy (SEM) image showing the mineral composition and microstructure of a typical shale sample (courtesy of C. Delle Piane). In this sample, the quartz (qz), calcite (cc), and pyrite (Pyr) grains are randomly distributed while the illite (Ill) shows some local disorder or misalignment, with respect to the vertical symmetry axis.

layer coating the surface of mineral grains) polarization [9] and neglects an important polarization mechanism in the intermediate frequency range (0.1 MHz–100 MHz), often referred to as Maxwell–Wagner polarization or interfacial polarization, due to the build-up of charge on the interfaces of the heterogeneous systems (e.g., [10]).

To describe the dielectric behaviors of a heterogeneous system caused by the Maxwell–Wagner polarization, various models have been developed (e.g., [11–20]) and a comprehensive review of the models can be found in Cai et al. [19]. Among these models, the differential effective medium (DEM) models are the kind of models that have had the most success in simulating the dielectric behavior of clay-free sedimentary rocks [21] and in modeling the high-frequency dielectric properties of both clay-free soils and clay soils [22]. The Hanai-Bruggeman (HB) equation [23–26] is one of such DEM models that predicts the bulk rock dielectric properties through the dielectric properties of the components, their volume fractions, and the geometric details of how the phases are arranged relative to each other described by the cementation factor (m). However, the HB model is designed for the isotropic medium only and could not be applied to modeling the anisotropic dielectric properties of shales. On the other hand, the Asami [27] model, as another kind of the DEM model, is capable of modeling the dielectric properties of a medium at any given direction relative to the applied electric field. The Asami model is a 2-phase (i.e., solid minerals and fluid) model that assumes that all the solid particles are uniformly shaped and aligned, which, however, is not the case for real shales that usually contain multiple mineral phases and the orientations of each of the minerals and the alignments of the different proportion of the same minerals are varying as shown in Figure 1. This requires the development of a multiphase anisotropic dielectric model where the complex mineral composition and the orientation distribution of the clay minerals can be accounted for; the model should also take into account the Stern layer polarization associated with clay minerals.

This work aims to present such a model. We first extend Asami's 2-phase anisotropic dielectric model to more phases based on an incremental algorithm [21, 28, 29] so that the multimineral nature of shales can be modeled. In the new model, the clay minerals with different orientations are grouped through the measured clay orientation distribution function, and the frequency dependent dielectric properties of the wet clay minerals that contain the information of the Stern layer polarization are determined by inverting the measured dielectric responses of an artificial sample composed of pure clay and pore water identical to that used in the shale under investigation with the silt component. The approach is then applied to modeling the laboratory measurements of the qualified samples in the frequency range 0.1 MHz–100 MHz presented in the companion paper.

2. Anisotropic Dielectric Model

2.1. Two-Phase Anisotropic Dielectric Model. Based on Maxwell–Wagner theory [30, 31], Asami [27] derived an equation for the complex relative permittivity (ε^*) of a 2-phase mixture where the ellipsoidal inclusions (with complex permittivity of ε_g^*) are oriented in the background medium (with complex permittivity of ε_a^*) with the angle φ_k between the k-axis and the electric field, as follows:

$$\varepsilon^* = \varepsilon_a^* \left[1 + \Phi \sum_{k=x,y,z} \frac{\varepsilon_g^* - \varepsilon_a^*}{\varepsilon_a^* + \left(\varepsilon_g^* - \varepsilon_a^*\right) L_k} \cos^2 \varphi_k \right], \quad (1)$$

where Φ is the volume fraction of the solid inclusions; the complex relative permittivity ε^* is defined as

$$\varepsilon^* = \varepsilon' - j\varepsilon'' = \varepsilon + \frac{\kappa}{j\varepsilon_0 \omega}, \quad (2)$$

where $j = \sqrt{-1}$, ε' and ε'' are the real and imaginary parts of ε^*, respectively, ε is the relative permittivity, κ is the effective conductivity, $\varepsilon_0 = 8.8542 \times 10^{-12}$ F/m is the absolute permittivity of vacuum, and $\omega = 2\pi f$ (where f is the frequency) is the angular frequency of the applied electric field. L_k is the k-axis depolarization factor of the oblate spheroidal inclusions ($R_x = R_y > R_z$, where R_k is the semiaxis of the ellipsoid along the k-axis) with aspect ratio $\alpha < 1$ ($\alpha = R_z/R_x$), given by [27]

$$\begin{aligned} L_z &= \frac{1}{1-\alpha^2} - \frac{\alpha}{\left(1-\alpha^2\right)^{3/2}} \cos^{-1}\alpha, \\ L_x &= L_y = \frac{\left(1 - L_z\right)}{2}. \end{aligned} \quad (3)$$

2.2. Multiphase Anisotropic Dielectric Model. Berg [21] presented an incremental algorithm to extend the 2-phase HB equation to more phases without ordering effect. Han et al. [28] adapted the algorithm to the isotropic dielectric model of Asami [27]. In this work, we apply the incremental concept to the 2-phase anisotropic dielectric model (see (1)) to enable more mineral components to be modeled.

In the new multiphase (M-phase) anisotropic dielectric model, the second phase with a volume fraction of C_2/n

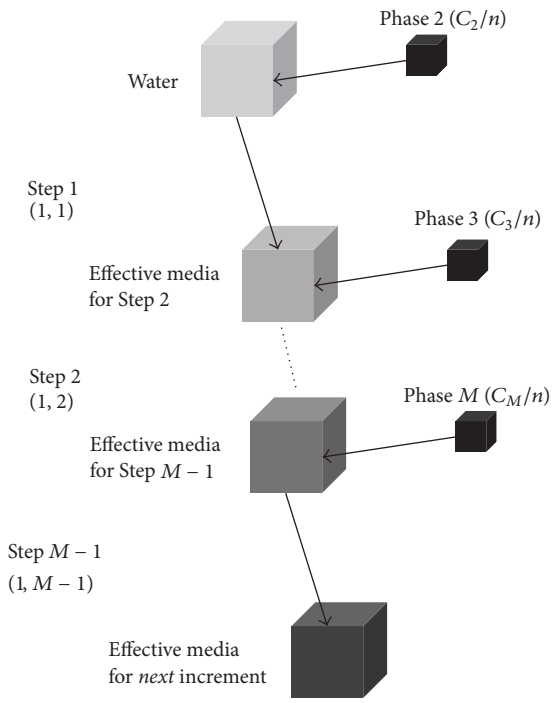

Figure 2: Schematic diagram showing the steps used in the first increment in the multiphase anisotropic dielectric model, in which water is the starting medium. The effective media formed in the last step of each increment become the starting background for the next increment, after Han et al. [28, 29].

(where C_2 is the initial concentration of phase 2 and n is the incremental number) is first added to the water (the first phase) background, forming an effective medium for the next step (step 2 as shown in Figure 2) in which phase 3 with a volume fraction of C_3/n is then included to form an effective background for step 3. This procedure continues until the Mth phase with volume fraction of C_M/n is finally added. The effective media formed when the $M-1$ phases included in each increment become a background for the next increment until the incremental number of n is reached. The effective media formed in each step are assumed to be an effective single phase, and the 2-phase anisotropic equation (see (1)) is used to calculate the effective dielectric properties in the directions parallel and perpendicular to the applied electric field, respectively.

In the incremental algorithm, the inclusion is added to the effective background to displace the same amount of medium; the volume fractions of the various phases in each step are therefore functions of their volume fractions in the previous step. Following Han et al. [28, 29], it is convenient to derive the volume fractions of the inclusions (V_i, $i = 1 : M$) based on their initial concentrations C and the incremental number n.

In the first increment (indicated by the column number), the volume fraction of each component after phase 2 is included (step 1, denoted by the row number):

$$V_1(1,1) = 1 - \frac{C_2}{n},$$

$$V_2(1,1) = \frac{C_2}{n},$$

$$V_3(1,1) = 0,$$

$$\vdots$$

$$V_M(1,1) = 0; \tag{4}$$

the volume fractions of the constituents when phase 3 is added (step 2) are calculated as

$$V_1(1,2) = V_1(1,1) \cdot \left(1 - \frac{C_3}{n}\right),$$

$$V_2(1,2) = V_2(1,1) \cdot \left(1 - \frac{C_3}{n}\right),$$

$$V_3(1,2) = \frac{C_3}{n}, \tag{5}$$

$$V_4(1,2) = 0,$$

$$\vdots$$

$$V_M(1,2) = 0;$$

the volume fractions of the components when phase 4 is added (step 3) are

$$V_1(1,3) = V_1(1,2) \cdot \left(1 - \frac{C_4}{n}\right),$$

$$V_2(1,3) = V_2(1,2) \cdot \left(1 - \frac{C_4}{n}\right),$$

$$V_3(1,3) = V_3(1,2)\cdot\left(1-\frac{C_4}{n}\right),$$
$$V_4(1,3) = \frac{C_4}{n},$$
$$V_5(1,3) = 0,$$
$$\vdots$$
$$V_M(1,3) = 0, \tag{6}$$

and after the final step (step $M-1$) when phase M is finally included in the first iteration, the volume fraction of each element can be found by

$$V_1(1,M-1) = V_1(1,M-2)\cdot\left(1-\frac{C_M}{n}\right),$$
$$\vdots$$
$$V_{M-1}(1,M-1) = V_{M-1}(1,M-2)\cdot\left(1-\frac{C_M}{n}\right), \tag{7}$$
$$V_M(1,M-1) = \frac{C_M}{n}.$$

The effective medium in the last step in each increment forms the starting background for the next increment; the volume fraction of each component in the ith increment ($2 \le i \le n$), after phases 2, 3, 4, and $M-1$ are added, is therefore given, respectively, by

$$V_1(i,1) = V_1(i-1,M-1)\cdot\left(1-\frac{C_2}{n}\right),$$
$$V_2(i,1) = V_2(i-1,M-1)\cdot\left(1-\frac{C_2}{n}\right)+\frac{C_2}{n},$$
$$V_3(i,1) = V_3(i-1,M-1)\cdot\left(1-\frac{C_2}{n}\right),$$
$$\vdots$$
$$V_M(i,1) = V_M(i-1,M-1)\cdot\left(1-\frac{C_2}{n}\right),$$
$$V_1(i,2) = V_1(i,1)\cdot\left(1-\frac{C_3}{n}\right),$$
$$V_2(i,2) = V_2(i,1)\cdot\left(1-\frac{C_3}{n}\right),$$
$$V_3(i,2) = V_3(i,1)\cdot\left(1-\frac{C_3}{n}\right)+\frac{C_3}{n},$$
$$V_4(i,2) = V_4(i,1)\cdot\left(1-\frac{C_3}{n}\right),$$
$$\vdots$$
$$V_M(i,2) = V_M(i,1)\cdot\left(1-\frac{C_3}{n}\right),$$
$$V_1(i,3) = V_1(i,2)\cdot\left(1-\frac{C_4}{n}\right),$$
$$V_2(i,3) = V_2(i,2)\cdot\left(1-\frac{C_4}{n}\right),$$
$$V_3(i,3) = V_3(i,2)\cdot\left(1-\frac{C_4}{n}\right),$$
$$V_4(i,3) = V_4(i,2)\cdot\left(1-\frac{C_4}{n}\right)+\frac{C_4}{n},$$
$$V_5(i,3) = V_5(i,2)\cdot\left(1-\frac{C_4}{n}\right),$$
$$\vdots$$
$$V_M(i,3) = V_M(i,2)\cdot\left(1-\frac{C_4}{n}\right),$$
$$V_1(i,M-1) = V_1(i,M-2)\cdot\left(1-\frac{C_M}{n}\right),$$
$$\vdots$$
$$V_{M-1}(i,M-1) = V_{M-1}(i,M-2)\cdot\left(1-\frac{C_M}{n}\right),$$
$$V_M(i,M-1) = V_M(i,M-2)\cdot\left(1-\frac{C_M}{n}\right)+\frac{C_M}{n}. \tag{8}$$

For a given rock sample with known volume fractions of the components (e.g., from laboratory measurements), the initial concentration of each phase for the model input can be determined from (4)–(8), based on the assigned incremental number n.

To demonstrate the effects of the order of mixing the different inclusions on the simulation results and their dependence on the iteration number n, we show in Figure 3 the modeling results for a hypothetical sample composed of brine (with relative permittivity and conductivity of 79 and 4.69 S/m, resp.) and 3 groups of quartz grains aligned 0°, 30°, and 90° to the bedding, respectively. The sample has a porosity of 0.1, and the quartz inclusions with alignment of 0°, 30°, and 90° to the bedding have volume fractions of 0.6, 0.2, and 0.1, respectively. The aspect ratios of all the quartz minerals are assumed to be 0.1, and the relative permittivity and conductivity are taken to be 20 and 10^{-5} S/m, respectively. In the example, the calculations at each iteration number are made using 6 different mixing orders of the 3 inclusions, as shown in the legend where 0, 30, and 90 stand for the quartz oriented 0°, 30°, and 90° to the bedding, respectively, and their orders in the legend represent the mixing order of the corresponding ingredients. The big separation between the simulated relative permittivity and conductivity when n is set to be 1 confirms that the conventional DEM model is dependent on the mixing order of the multiple components (e.g., [15, 32, 33]). With an increase in the iteration number, the ordering effect decreases, and the calculated relative permittivity and conductivity at each direction start to converge and become identical when the iteration number

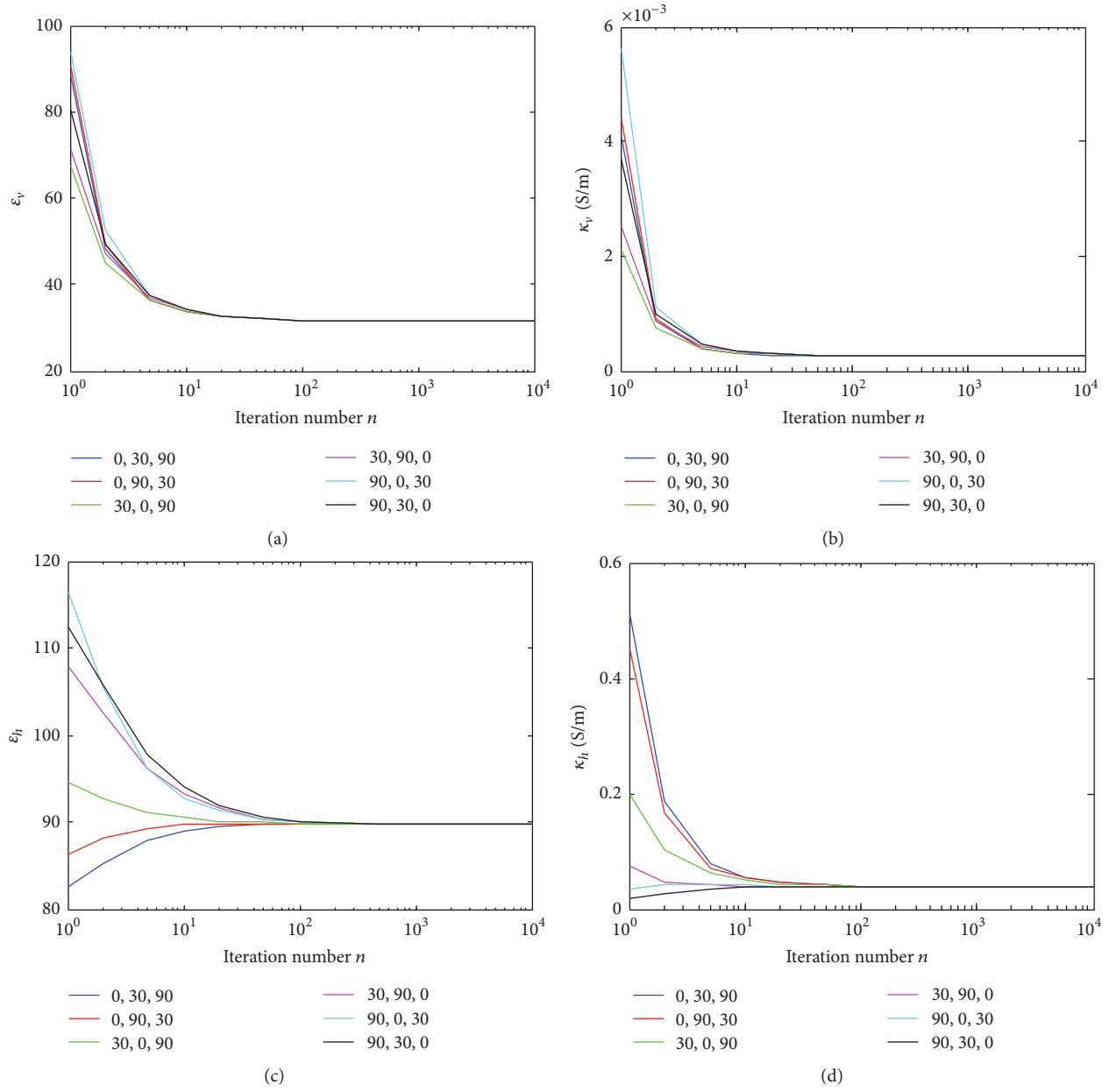

FIGURE 3: Simulated relative permittivity and conductivity of the hypothetical sample in the directions when the applied electric field is perpendicular (ε_v and κ_v, resp.) and parallel (ε_h and κ_h, resp.) to the bedding, respectively. The lines with varying colors are for the quartz grains with different mixing orders, where 0, 30, and 90 stand for the quartz oriented 0°, 30°, and 90° to the bedding, respectively.

is sufficiently high (i.e., when $n = 1000$), demonstrating that the developed multiphase anisotropic dielectric model is independent of mixing order at high iteration numbers. A further increase in the iteration number will not affect the results but may cause an increase in the computing time. Therefore, unless otherwise stated, an iteration number of 1000 is used for the rest of the calculations to guarantee accuracy of the simulation results in a quick manner.

3. Application to Artificial Shales

3.1. Sample Selection. Having developed the multiphase anisotropic dielectric model, we proceed to apply the model to simulating the laboratory measured frequency dependent dielectric responses of the artificial shales presented in the companion paper. To do this, as mentioned previously, the frequency dependent dielectric properties of the rock-forming components, their volume fractions, and geometric information are needed as the inputting model parameters. While the dielectric properties of the insulating silt and the conductive water can be regarded frequency independent in the frequency range between 0.1 MHz and 100 MHz, there is evidence that the dielectric properties of wet clay minerals are frequency dependent as a result of the Stern layer polarization associated with clay minerals (e.g., [34]). Since the magnitude of the Stern layer polarization depends on the water salinity,

Table 1: Volume fractions of the rock-forming components for the model input of the 3 samples under investigation. The volume fractions are determined based on the measured sample porosity, the solid silt to kaolinite ratio, and the obtained orientation distribution function of the kaolinite grains.

Sample	φ	V_{silt}	V_{kao}^{0}	V_{kao}^{30}	V_{kao}^{60}	V_{kao}^{90}
A0100_75	0.18	0	0.4756	0.2303	0.0682	0.0459
A2575_75	0.158	0.2105	0.4111	0.1792	0.0285	0.0127
A4060_75	0.14	0.3440	0.2893	0.1614	0.0429	0.0224

the dielectric properties of wet clay minerals are also related to the properties of water. It is therefore reasonable to select a series of samples (in disc shape with diameter of 20 mm and thickness of 3–5 mm) saturated with the same brine but with varying clay to silt ratios so that the frequency dependent dielectric properties of the wet clay minerals at this specific brine conditions can be inverted based on the developed model from the measured dielectric behaviors of the sample with no silt fraction (i.e., the sample composed of only kaolinite and brine). Samples fulfilling this criterion include the dispersed samples saturated with distilled water (i.e., samples D0100_0 and D4555_0) and the aggregated samples filled with 75 g/l KCl brine (i.e., samples A0100_75, A2575_75, and A4060_75). Considering the fact that the contributions to the dielectric responses of the distilled water saturated shales are mainly from the Stern layer polarization which overwhelms the Maxwell–Wagner polarization, based on which the multiphase dielectric model is developed, therefore, only the aggregated shales samples saturated with 75 g/l KCl are selected for the modeling.

3.2. Determination of the Volume Fractions of the Ingredients. We use the measured porosity, preset silt to kaolinite weight ratios, and the collected orientation distributions of the kaolinite grains (as shown in Figure 4 for all the 3 samples in consideration) to determine the volume fractions of the ingredients, which are essential for the model inputs. The clay particle orientation distributions are measured using neutron diffraction goniometry at polar angle interval of 5°, giving rise to 19 data points in the range 0° to 90°. Although the multiphase model is developed for any number of phases, the 19 clay phases will significantly increase the computing time. To simplify the clay orientation distributions but to keep the effects of the distribution density on the dielectric anisotropy, we choose 4 representative angles instead of using the complete orientation distributions. This is done by averaging the obtained distribution densities, respectively, between 0° and 15°, 20° and 40°, 50° and 70°, and 75° and 90° to represent the orientation distributions at 0°, 30°, 60°, and 90°, respectively. Considering the fact that kaolinite and silt grains are similar in densities (the densities of the kaolinite and quartz were determined to be 2.61 g/cm^3 and 2.65 g/cm^3, respectively), the volume fractions of the kaolinite at the 4 polar angles (V_{kao}^{i}) and the volume fraction of the silt (V_{silt}) are then determined as

$$V_{\text{kao}}^{i} = (1-\varphi)\, W_{\text{kao}} \frac{d_{\text{kao}}^{i}}{\sum_{i=0,30,60,90} d_{\text{kao}}^{i}}, \qquad (9)$$
$$V_{\text{silt}} = (1-\varphi)\, W_{\text{silt}},$$

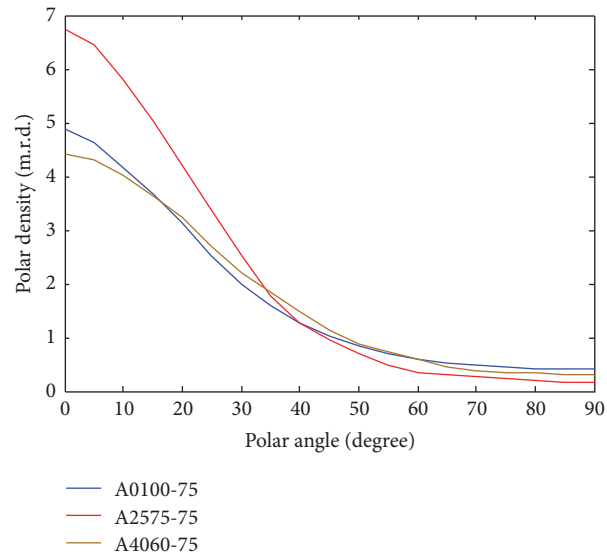

Figure 4: Experimental c-axis distribution density figures of the kaolinite in the 3 samples with corresponding integrated polar angle profiles. Distribution density is expressed in multiples of random distribution (m.r.d.).

where φ is the porosity of the artificial shale sample, W_{silt} and W_{kao} are the preset weight ratio between silt and kaolinite, and d_{kao}^{i} are the averaged orientation distribution densities at 0°, 30°, 60°, and 90°, respectively.

The calculated volume fractions of the ingredients for all the 3 samples are listed in Table 1, and the initial concentrations of the various phases C that are directly input into the model can be obtained from (4)–(8), based on the assigned incremental number $n = 1000$.

3.3. Inversion of the Dielectric Properties of Wet Clays. To obtain the unknown dielectric properties of the wet clay minerals that are dependent on the brine (among many other factors including grain size and temperature) saturating the shale samples, we invert the measured dielectric behaviors of the artificial sample made of pure kaolinite and the same brine filling the other 2 samples, that is, the 75 g/l KCl brine with relative permittivity of 79 and electrical conductivity of 11.2 S/m. The inversion is done on sample A0100_75 by minimizing the difference between the laboratory measurements and the model prediction for relative permittivity and conductivity in the directions parallel and perpendicular to the bedding, respectively, at each frequency between 0.1 MHz and 100 MHz where the laboratory data are collected. In the

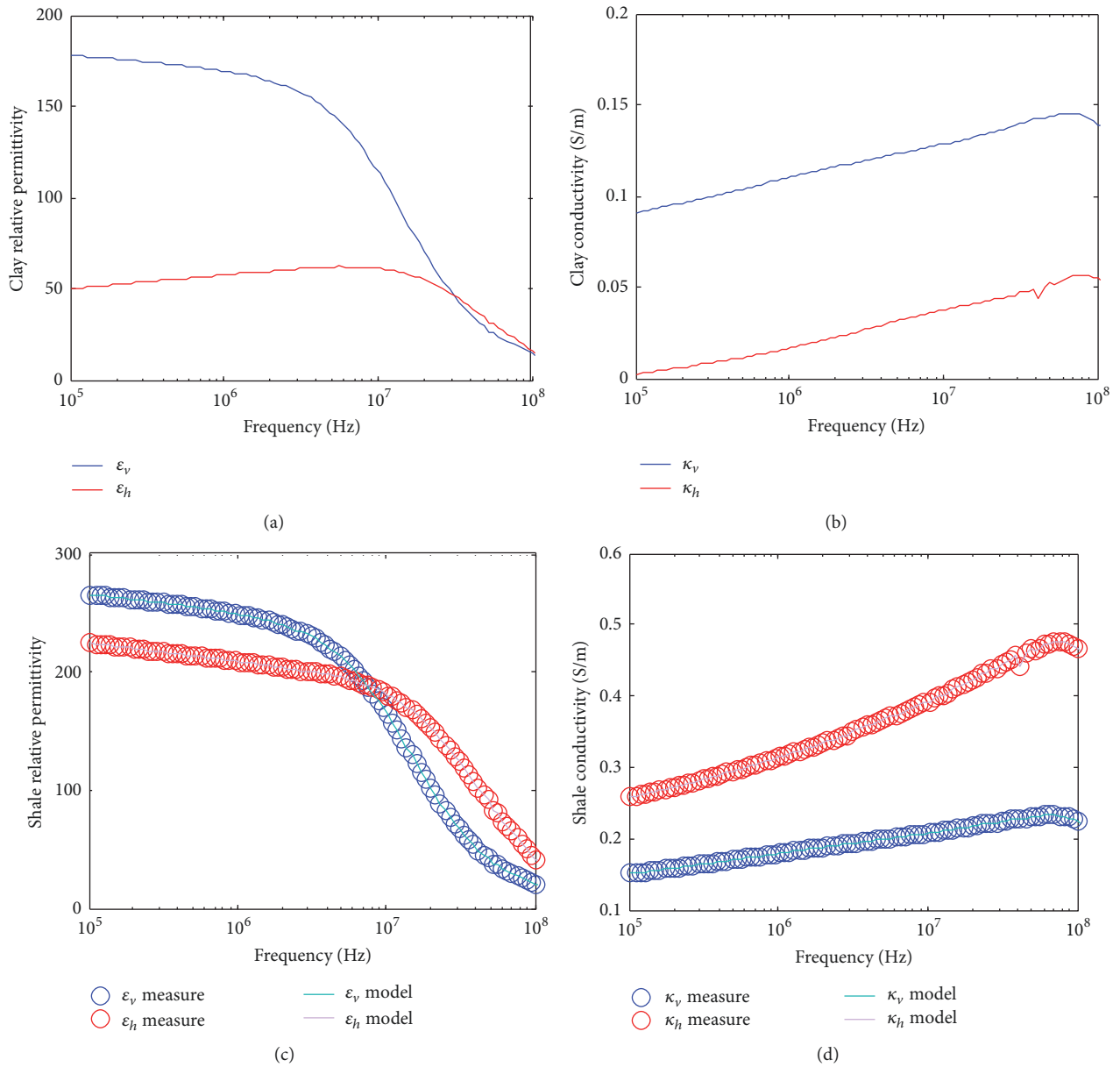

FIGURE 5: Inverted frequency dependent relative permittivity (a) and conductivity (b) of the wet kaolinite and comparison of the laboratory measured relative permittivity (c) and conductivity (d) of the shale sample A0100_75 with the model prediction based on the wet kaolinite properties in the vertical and horizontal directions, respectively.

modeling, an aspect ratio of 0.1 is employed for the kaolinite grains based on analysis of the SEM images of the compacted sample [35].

The results are given in Figure 5 for the inverted frequency dependent relative permittivity and electrical conductivity of the wet kaolinite in the vertical (perpendicular to the bedding, in blue curves) and horizontal (parallel to the bedding, in red curves) directions, respectively. Also shown in Figure 5 is the comparison of the measured shale (A0100_75) relative permittivity and conductivity (vertical and horizontal, resp.) with those predicted using the developed anisotropic model based on the inverted wet clay dielectric properties and their simplified orientation distributions.

The wet clay dielectric properties obtained in the vertical and horizontal directions are for the brine coated oblate kaolinite grains in the directions along the short and long axis, respectively. These properties are thought to be a result of the Stern layer polarization only that is dependent merely on the brine properties and are assumed to be the properties of the wet clay in the artificial shales saturated with the same brine. The anisotropic wet clay dielectric properties are further employed to account for the Maxwell–Wagner polarization through the developed multiphase model to predict the anisotropic dielectric behaviors of the shales with varying amounts of silt fractions. It should be noted that the excellent agreement between the laboratory data and the

model prediction as shown in Figures 5(c) and 5(d) is not an indication of the correctness of either the new model or the inverted wet clay dielectric properties but does imply that the combination of them can sufficiently simulate the measured frequency dependent dielectric behaviors of the silt-free shale sample. It is therefore reasonable to expect that the joint employment of the developed model and the obtained wet clay dielectric properties could also give satisfactory simulation to the artificial samples with the silt fractions, as to be shown in the next section.

3.4. Modeling Results. Having selected qualified artificial shale samples, having determined the volume fractions of their ingredients, and having obtained the frequency dependent dielectric properties of wet kaolinite clay aggregates form a basis for the developed multiphase model to simulate the measured anisotropic responses of the shale samples with silt fractions, which makes the artificial samples more resembling natural shales in terms of their mineral compositions. The inclusion of the silt fractions, however, will add additional complexity to the model.

Firstly, the distribution of the silt fractions turns to be random in the kaolinite matrix, making the shale less anisotropic. To adjust the developed multiphase anisotropic dielectric model to be capable of adding isotropic inclusions, the 2-phase anisotropic dielectric model (see (1)) is replaced with the 2-phase isotropic model when the silt component is added, given as follows [27]:

$$\varepsilon^* = \varepsilon_a^* \left[1 + \frac{1}{3}\Phi \sum_{k=x,y,z} \frac{\varepsilon_g^* - \varepsilon_a^*}{\varepsilon_a^* + \left(\varepsilon_g^* - \varepsilon_a^*\right) L_k} \right]. \quad (10)$$

Secondly, the dielectric properties of wet silt are unknown. It is well documented in the literature that dry quartz mineral has a relative permittivity of approximately 4.5 (e.g., [36]), but wet quartz exhibits higher values due to the electrochemical interactions of the mineral-water system. In this work, a constant relative permittivity of 20 [37, 38] is employed for wet silt with an electrical conductivity of 10^{-5} S/m. The high relative permittivity value for the wet silt can be explained by the polarization at the mineral-water surface and/or by the fact that there are small amount of silt grains with high aspect ratio, which give rise to high relative permittivity at relative low frequencies [39]. And lastly, the geometric information (i.e., aspect ratio) of the silt fractions that is required for the model input needs to be determined. In this work, the silt aspect ratio is set as a fitting parameter to give the best correlation coefficient between laboratory measurements (both relative permittivity and conductivity) and model prediction in the vertical and horizontal directions, respectively.

Using the dielectric properties of the various ingredients together with their volume fractions (as listed in Table 1) and aspect ratios, the built anisotropic multiphase dielectric model is applied to the artificial shale samples of A2575_75 and A4060_75 based on the procedures outlined above.

The modeling results for the artificial shale sample A2575_75 are given in Figure 6. By using the silt aspect ratios of 0.1 and 0.06 the modeled dielectric responses give satisfactory fit to the dielectric measurements at the vertical and horizontal directions, respectively, with correlation coefficients of $R = 0.9833$ and $R = 0.9775$ for the relative permittivity and conductivity in the vertical direction and $R = 0.9979$ and $R = 0.9940$ for the relative permittivity and conductivity in the horizontal direction, respectively. The obtained silt aspect ratios of 0.1 and 0.06 are within the aspect ratio range of the silt from the micro-CT image of the compacted sample [35] and can also be explained by the nonhomogeneous microstructure at the sample scale [40]. It is interesting that different values of the silt aspect ratio are inverted in the orthogonal directions and this can be explained by the fact that although randomly dispersed silts are assumed in the model, they are in fact aligned to some extent, and therefore their contributions to the dielectric responses at different directions are varying; as a result, different values for the silt grain aspect ratio should be used. This is similar to the distinct wet clay dielectric properties that are employed to model the anisotropic shale properties in the different directions.

Figure 7 shows the modeling results for the sample A4060_75. When the silt grain aspect ratio is determined to be 0.1 for both vertical and horizontal directions, the new multiphase anisotropic dielectric model gives best fit to the laboratory measurements with correlation coefficients of $R = 0.9921$ and $R = 0.9433$ for the vertical relative permittivity and conductivity and $R = 0.9971$ and $R = 0.9943$ for the relative permittivity and conductivity horizontally, respectively. The inverted silt aspect ratio is consistent with the results obtained for the sample A2575_75 with less silt content and the uniform silt aspect ratio for the orthogonal directions indicates that the silt grains are more homogeneously distributed in the sample so that the dielectric properties of the rock caused by the silt component can by effectively described by the isotropic model (see (10)).

4. Discussion

The multiphase anisotropic dielectric model was developed based on the incremental algorithm [21, 28], in which a small amount of each component is required to be added in every increment, making the model independent of the mixing order, a problem usually encountered by multiphase DEM models [15, 32, 33]. This excludes the difference in the results caused by the order of mixing the different mineral phases and ensures that the results are unique for the determined shale dielectric properties based on the dielectric responses and volume fractions of the constituents and their specific microstructure described by the simplified orientation distribution function of the clay particles, which determines the anisotropy of the bulk dielectric properties through the orientational alignments of the clay minerals. A complete orientation distribution of the clay minerals as measured may give better anisotropic results for the model, but will also increase dramatically the computing time due to the repeated incremental addition of the more directional phases. It turns out that the simplified clay orientation distribution function as proposed above is a reasonable s compromise that gives excellent model to laboratory data fit at relatively lower simulation costs.

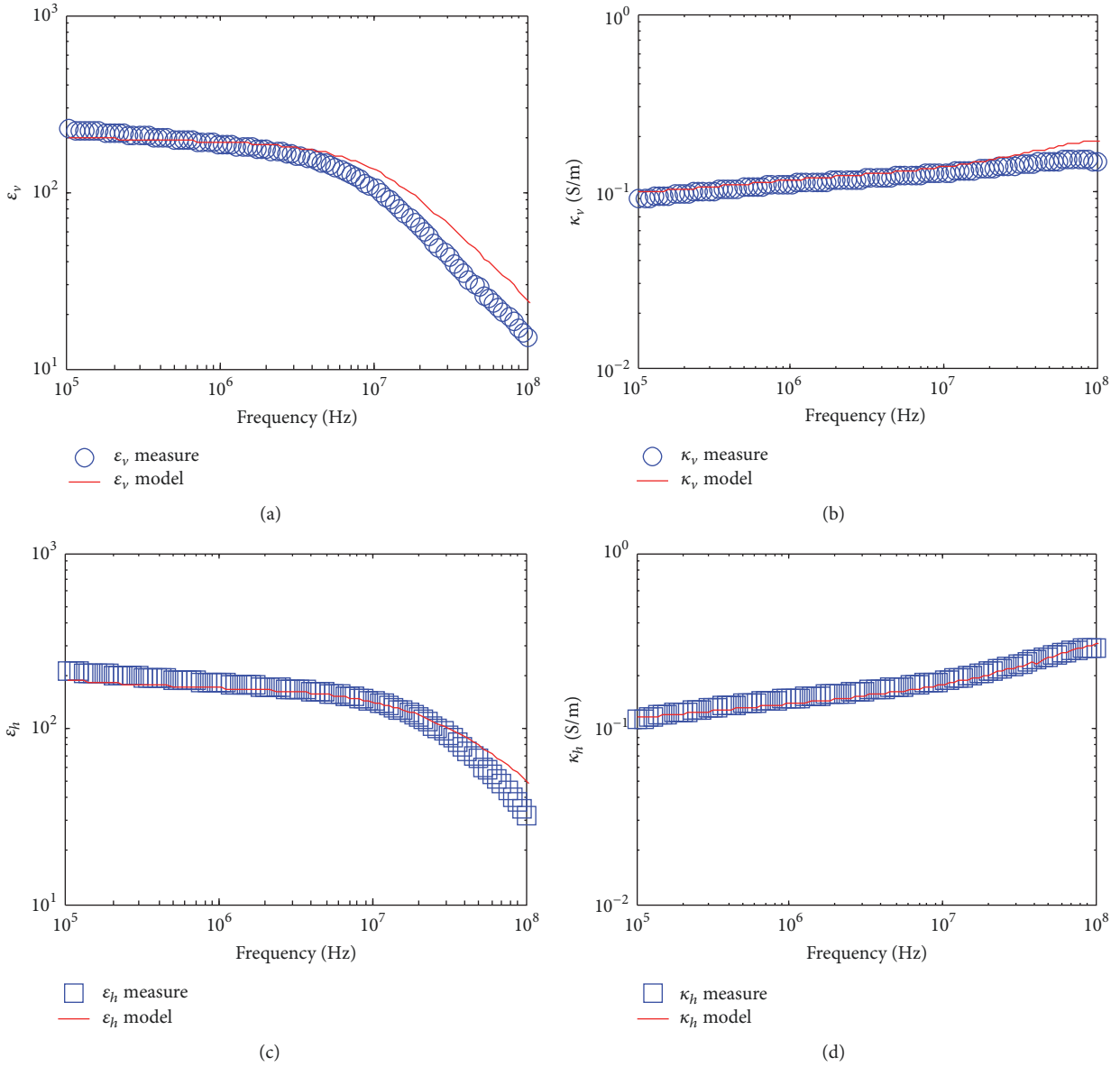

FIGURE 6: Comparison of the experimental measurements with the modeling results for the artificial shale sample A2575_75. The correlation coefficients are $R = 0.9833$ and $R = 0.9775$, respectively, for the relative permittivity and conductivity in the vertical direction and $R = 0.9979$ and $R = 0.9940$ for the relative permittivity and conductivity in the horizontal direction, respectively.

The direction dependent dielectric properties of the wet clay aggregates as a function of frequency are inverted from the silt-free artificial shale sample using the built multiphase dielectric model. Since the Maxwell–Wagner polarization has already been accounted for by the new model, the obtained anisotropic dielectric properties of the wet clay minerals are thought to be the results of all other types of polarization mechanisms including the Stern layer polarization in the directions along the axes of the clay particles coated by the specific 75 g/l KCl brine. The obtained wet clay dielectric properties can be validated by the models based on Stern layer polarization (e.g., [34]); however such models usually need additional parameters (e.g., formation factor and cation exchange capacity of the sample and electrochemical properties of the pore filling brine) which are not available from the experiments presented in the companion paper. Nevertheless, as mentioned in the context, through the inverted wet clay dielectric properties, the proposed modeling approach combines the Stern layer and Maxwell–Wagner polarization mechanisms in the intermediate frequency range 0.1 MHz–100 MHz, which is a clear advantage of the model over other theoretical models that deal with only one of the polarization mechanisms.

In addition to the anisotropic dielectric properties of the wet clay minerals, the shale dielectric anisotropy in the modeling is caused exclusively by the aligned clay minerals and the silt grains are assumed to be randomly dispersed, which leads to isotropic dielectric properties if the background is

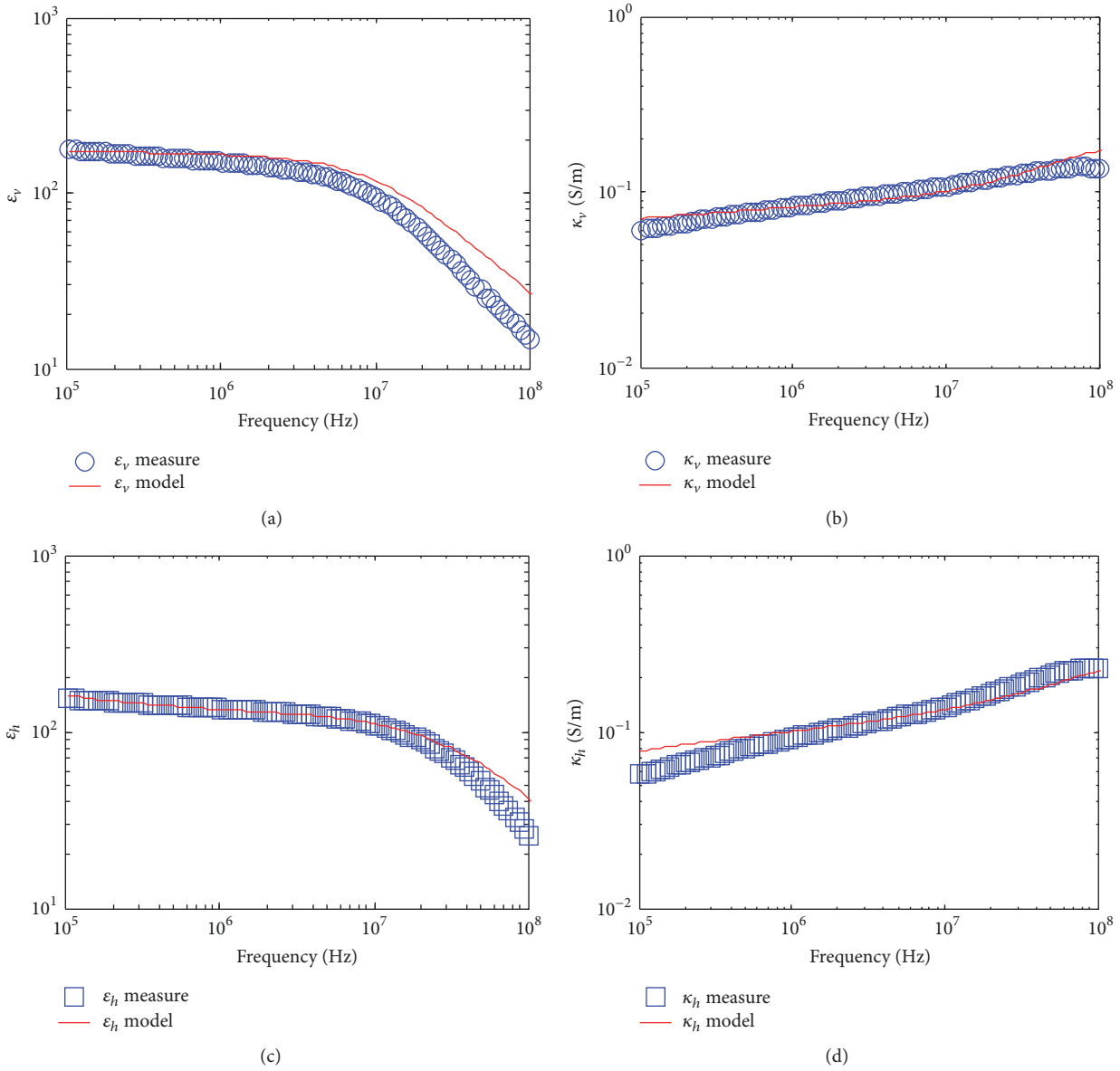

FIGURE 7: Comparison of the experimental measurements with the modeling results for the artificial shale sample A4060_75. The correlation coefficients are $R = 0.9921$ and $R = 0.9433$, respectively, for the relative permittivity and conductivity in the vertical direction and $R = 0.9971$ and $R = 0.9943$ for the relative permittivity and conductivity in the horizontal direction, respectively.

homogeneous and reduces anisotropy if the host matrix is anisotropic. The 2-phase isotropic model [27] is therefore employed to account for the dielectric properties when the silt fractions are included. However, the different silt aspect ratios obtained from the inversion for sample A2575_75 of the 2 orthogonal directions indicates that the contributions of the silt grains to the bulk dielectric behaviors are dependent on the directions, which in turn implies that the silt grains are not randomly distributed as assumed, which will originate additional anisotropy to the sample [40]. A detailed laboratory investigation of the orientation distribution of the silt grains is needed to enable the developed multiphase model to better simulate the anisotropic dielectric properties of shales, and this will be one of the topics for a future study.

The wet clay dielectric properties are frequency dependent in the modeling, while the relative permittivity and conductivity of the wet silt grains are assumed to be constant over the frequency range under investigation. It should be noted, however, that the dielectric responses of wet quartz should also be a function of the applied electrical field frequency, due to the electrochemical interactions of the mineral-water system that give additional contribution to the rock dielectric properties [6, 37, 38]. To better determine the frequency dependent dielectric properties of the wet silt, a separate experiment measuring the relative permittivity and conductivity of the silt and 75 g/l KCl brine mixture as a function of frequency is needed, and an inversion algorithm as presented in the context to obtain the frequency dependent

dielectric properties of the wet clay minerals can be implemented to remove the effects caused by the Maxwell–Wagner polarization to finally arrive at the dependence of the wet silt dielectric properties on frequency that is a result merely of the Stern layer polarization. The derived relative permittivity and conductivity of the wet silt are essentially the effective values resulting from the electrochemical Stern layer polarization at each frequency [41].

The proposed modeling approach can be applied to calibrating and comparing the results of different geophysical methods that acquire the dielectric properties from different directions (i.e., dielectric logging from the horizontal direction and surface Induced Polarization method from the vertical direction) in addition to determining the geofluids type and concentration and estimating the transport properties of the shales. Another important potential application of the modeling is for the detection and prediction of overpressure in shales due to their extremely low permeability that makes the pore pressure less able to equilibrate to hydrostatic pressure. Accurate overpressure detection and prediction play an important role in understanding the depositional and evolutional history of a sedimentary basin, hydrocarbon migration, and trapping in the reservoir, as well as in reducing the risks of drilling hazards during hydrocarbon exploitation [42–45]. Overpressure results in lower than expected electrical resistivity (reciprocal of conductivity) through the enlarged porosity associated with the high pore pressure, and conventional overpressure prediction models based on electrical properties evaluate the difference between the measured electrical properties and those of the normally compacted shales at the same depth to estimate the abnormal pore pressure [46, 47]. Since the developed multiphase dielectric model does not take into account the pressure effects, the modeled shale electrical properties can then be regarded as the electrical properties of the shales if the pore pressure is normal (i.e., the normally compacted shale electrical properties), which can be further employed for the overpressure prediction based on their difference from the measured electrical anomalies. Application of the multiphase model to the overpressure detection and prediction in shales will be a topic for a future study.

5. Conclusions

A multiphase incremental model has been developed for the anisotropic dielectric properties of sedimentary rocks. The model is for any number of mineral grain components aligned in any direction and is independent of the mixing order. Based on the new model, we propose a modeling approach for the frequency dependent anisotropic dielectric properties of shales in which the shale anisotropy is determined from the measured orientation distribution function of the clay particles and the dielectric properties of the wet clay minerals are inverted from the obtained dielectric behaviors of the artificial shale sample composed of clay and brine that is the same as that used in other shale samples. The method combines the two important polarization mechanisms (i.e., the Stern layer polarization and the Maxwell–Wagner polarization, resp.) taking effect in the intermediate frequency range of 0.1 MHz–100 MHz. Application of the modeling approach to the artificial shale samples with varying silt contents show that the frequency dependent relative permittivity and conductivity of the shales in the two orthogonal directions can be satisfactorily modeled by using a reasonable aspect ratio and constant dielectric parameters for the silt grains.

Conflicts of Interest

The authors declare that they have no conflicts of interest.

Acknowledgments

The authors would like to thank the CSIRO Shale Rock Physics and Petrophysics (SHARPP) project sponsored by Total and the Strategic Research Program of the Chinese Academy of Sciences (XDA14010303) for financial support of this work.

References

[1] C. Clavier, G. Coates, and J. Dumanoir, "Theoretical and experimental bases for the dual-water model for interpretation of shaly sands," *SPE Journal*, vol. 24, no. 2, pp. 153–168, 1984.

[2] O. A. L. De Lima and M. M. Sharma, "A grain conductivity approach to shaly sandstones," *Geophysics*, vol. 55, no. 10, pp. 1347–1356, 1990.

[3] P. W. Glover, P. G. Meredith, P. R. Sammonds, and S. A. Murrell, "Ionic surface electrical conductivity in sandstone," *Journal of Geophysical Research: Solid Earth*, vol. 99, no. B11, pp. 21635–21650, 1994.

[4] A. Rabaute, A. Revil, and E. Brosse, "In situ mineralogy and permeability logs from downhole measurements: application to fa case study in chlorite-coated sandstones," *Journal of Geophysical Research: Atmospheres*, vol. 108, no. 108, pp. 369–378, 2003.

[5] P. Leroy, A. Revil, A. Kemna, P. Cosenza, and A. Ghorbani, "Complex conductivity of water-saturated packs of glass beads," *Journal of Colloid and Interface Science*, vol. 321, no. 1, pp. 103–117, 2008.

[6] A. Revil and M. Skold, "Salinity dependence of spectral induced polarization in sands and sandstones," *Geophysical Journal International*, vol. 187, no. 2, pp. 813–824, 2011.

[7] N. Schwartz and A. Furman, "Spectral induced polarization signature of soil contaminated by organic pollutant: experiment and modeling," *Journal of Geophysical Research: Atmospheres*, vol. 117, no. B10, Article ID B10203, 10203 pages, 2012.

[8] A. Revil, W. F. Woodruff, C. Torres-Verdín, and M. Prasad, "Complex conductivity tensor of anisotropic hydrocarbon-bearing shales and mudrocks," *Geophysics*, vol. 78, no. 6, pp. D403–D418, 2013.

[9] O. Stern, "Zur theorie der electrolytischen doppelschicht (the theory of the electrolytic double shift)," *Zeitschrift Fur Elektrochemie Und Angewandte Physikalische Chemie*, vol. 30, pp. 508–516, 1924.

[10] L. K. H. van Beek, "Dielectric behaviour of heterogeneous systems," in *Progress in Dielectrics*, vol. 7, pp. 69–114, Heywood Books, London, 1967.

[11] P. N. Sen C. Scala and M. H. Cohen, "A self-similar model for sedimentary rocks with application to the dielectric constant of fused glass beads.," *Geophysics*, vol. 46, no. 5, pp. 781–795, 1981.

[12] J. G. Berryman, "Mixture theories for rock properties," in *Rock Physics & Phase Relations*, vol. 3, pp. 205–228, American Geophysical Union, Washington, D. C., USA, 1995.

[13] L.-J. Gelius and Z. Wang, "Modelling production caused changes in conductivity for a siliciclastic reservoir: a differential effective medium approach," *Geophysical Prospecting*, vol. 56, no. 5, pp. 677–691, 2008.

[14] M. H. Ellis, M. C. Sinha, T. A. Minshull, J. Sothcott, and A. I. Best, "An anisotropic model for the electrical resistivity of two-phase geologic materials," *Geophysics*, vol. 75, no. 6, pp. E161–E170, 2010.

[15] T. Han, A. I. Best, L. M. MacGregor, J. Sothcott, and T. A. Minshull, "Joint elastic-electrical effective medium models of reservoir sandstones," *Geophysical Prospecting*, vol. 59, no. 4, pp. 777–786, 2011.

[16] J. G. Berryman and G. M. Hoversten, "Modelling electrical conductivity for earth media with macroscopic fluid-filled fractures," *Geophysical Prospecting*, vol. 61, no. 2, pp. 471–493, 2013.

[17] P. W. J. Glover, "A generalized Archie's law for n phases," *Geophysics*, vol. 75, no. 6, pp. E247–E265, 2010.

[18] W. Wei, J. Cai, X. Hu, and Q. Han, "An electrical conductivity model for fractal porous media," *Geophysical Research Letters*, vol. 42, no. 12, pp. 4833–4840, 2015.

[19] J. Cai, W. Wei, X. Hu, and D. A. Wood, "Electrical conductivity models in saturated porous media: a review," *Earth-Science Reviews*, vol. 171, pp. 8419–8433, 2017.

[20] P. N. Sævik, M. Jakobsen, M. Lien, and I. Berre, "Anisotropic effective conductivity in fractured rocks by explicit effective medium methods," *Geophysical Prospecting*, vol. 62, no. 6, pp. 1297–1314, 2014.

[21] C. Berg, "An effective medium algorithm for calculating water saturations at any salinity or frequency," *Geophysics*, vol. 72, no. 2, pp. E59–E67, 2007.

[22] P. Cosenza, C. Camerlynck, and A. Tabbagh, "Differential effective medium schemes for investigating the relationship between high-frequency relative dielectric permittivity and water content of soils," *Water Resources Research*, vol. 39, no. 9, 1230 pages, 2003.

[23] D. A. Bruggeman, "Berechnung verschiedener physikalischer Konstanten von heterogenen Substanzen," *Annalen der Physik*, vol. 416, no. 7, pp. 636–664, 1935.

[24] T. Hanai, "Theory of the dielectric dispersion due to the interfacial polarization and its application to emulsions," *Colloid and Polymer Science*, vol. 171, no. 1, pp. 23–31, 1960.

[25] T. Hanai, "A remark on the "Theory of the dielectric dispersion due to the interfacial polarization"," *Colloid and Polymer Science*, vol. 175, no. 1, pp. 61-62, 1961.

[26] A. E. Bussian, "Electrical conductance in a porous medium.," *Geophysics*, vol. 48, no. 9, pp. 1258–1268, 1983.

[27] K. Asami, "Characterization of heterogeneous systems by dielectric spectroscopy," *Progress in Polymer Science*, vol. 27, no. 8, pp. 1617–1659, 2002.

[28] T. Han, M. B. Clennell, M. Josh, and M. Pervukhina, "Determination of effective grain geometry for electrical modeling of sedimentary rocks," *Geophysics*, vol. 80, no. 4, pp. D319–D327, 2014.

[29] T. Han, M. B. Clennell, and M. Pervukhina, "Modelling the low-frequency electrical properties of pyrite-bearing reservoir sandstones," *Marine and Petroleum Geology*, vol. 68, pp. 341–351, 2015.

[30] J. C. Maxwell, *Treatise on electricity and magnetism*, The Clarendon Press, Oxford University Press, 1891.

[31] K. W. Wagner, "Erklärung der dielektrischen Nachwirkungsvorgänge auf Grund Maxwellscher Vorstellungen," *Archiv für Elektrotechnik*, vol. 2, no. 9, pp. 371–387, 1914.

[32] M. Spalburg, "The effective medium theory used to derive conductivity equations for clean and shaly hydrocarbon-bearing reservoirs," in *Proceedings of the 11th European Formation Evaluation Symposium*, 1988.

[33] P. Cosenza, A. Ghorbani, C. Camerlynck, F. Rejiba, R. Guérin, and A. Tabbagh, "Effective medium theories for modelling the relationships between electromagnetic properties and hydrological variable in geomaterials: a review," *Near Surface Geophysics*, vol. 7, no. 5-6, pp. 563–578, 2009.

[34] A. Revil, "On charge accumulation in heterogeneous porous rocks under the influence of an external electric field," *Geophysics*, vol. 78, no. 4, pp. D271–D291, 2013.

[35] R. Beloborodov, M. Pervukhina, V. Luzin et al., "Compaction of quartz-kaolinite mixtures: the influence of the pore fluid composition on the development of their microstructure and elastic anisotropy," *Marine and Petroleum Geology*, vol. 78, pp. 426–438, 2016.

[36] G. R. Olhoeft, "Electrical properties of rocks," in *Physical Properties of Rocks and Minerals*, pp. 257–329, Hemisphere Publishing Corporation, Now York, NY, USA, 1989.

[37] J. L. Davis and A. P. Annan, "Ground-penetrating radar for high-resolution mapping of soil and rock stratigraphy," *Geophysical Prospecting*, vol. 37, no. 5, pp. 531–551, 1989.

[38] D. J. Daniels, "Surface-penetrating radar—IEE Radar, Sonar, Navigation and Avionics Series 6," *The Institue of Electrical Engineers*, 1996, London, UK.

[39] P. N. Sen, "Relation of certain geometrical features to the dielectric anomaly of rocks," *Geophysics*, vol. 46, no. 12, pp. 1714–1720, 1981.

[40] P. Cosenza, D. Prêt, and M. Zamora, "Effect of the local clay distribution on the effective electrical conductivity of clay rocks," *Journal of Geophysical Research: Solid Earth*, vol. 120, no. 1, pp. 145–168, 2015.

[41] O. A. L. De Lima and M. M. Sharma, "A generalized Maxwell-Wagner theory for membrane polarization in shaly sands," *Geophysics*, vol. 57, no. 3, pp. 431–440, 1992.

[42] B. J. O. L. Mcpherson and G. Garven, "Hydrodynamics and overpressure mechanisms in the Sacramento basin, California," *American Journal of Science*, vol. 299, no. 6, pp. 429–466, 1999.

[43] A. Muggeridge and H. Mahmode, "Hydrodynamic aquifer or reservoir compartmentalization?" *AAPG Bulletin*, vol. 96, no. 2, pp. 315–336, 2012.

[44] M. R. P. Tingay, R. R. Hillis, R. E. Swarbrick, C. K. Morley, and A. R. Damit, "Origin of overpressure and pore-pressure prediction in the Baram province, Brunei," *AAPG Bulletin*, vol. 93, no. 1, pp. 51–74, 2009.

[45] T. Han, M. Pervukhina, M. B. Clennell, and D. N. Dewhurst, "Model-based pore-pressure prediction in shales: an example from the gulf of Mexico, North America," *Geophysics*, vol. 82, no. 3, pp. M37–M42, 2017.

[46] C. Hottmann and R. Johnson, "Estimation of formation pressures from log-derived shale properties," *Journal of Petroleum Technology*, vol. 17, no. 06, pp. 717–722, 1965.

[47] J. Zhang, "Pore pressure prediction from well logs: methods, modifications, and new approaches," *Earth-Science Reviews*, vol. 108, no. 1-2, pp. 50–63, 2011.